Soft Matter

Accepted Manuscript

ROYAL SOCIETY OF CHEMISTRY

rsc.li/soft-matter-journal

View Article Online
DOI: 10.1039/D5SM00841G

Soft Matter

ARTICLE TYPE

Cite this: DOI: 00.0000/xxxxxxxxxx

Lifetime and fluctuations of specific bonds between anisotropic colloids mediated through depletion interactions.

M Mayarani,*[a,b,c], Justine Laurent [d], Martin Lenz,[a,b], Olivia du Roure[a*] and Julien Heuvingh[a]

Received Date
Accepted Date

DOI: 00.0000/xxxxxxxxxx

To fabricate large-scale structures using colloidal particle self-assembly, one of the main challenges is to prevent kinetic trapping in metastable states. Therefore, interactions and colloids must be carefully chosen to ensure selectivity to guide the assembly, reversibility to enable large-scale reorganization and flexibility to finely tune colloid positioning. In pursuit of this, we study simple anisotropic colloids in the shape of half-disks fabricated using two-photon lithography and drive their self-assembly trough their vertical faces using depletion interactions. Depletion interactions are widely used in the literature to induce colloidal self-assembly and can provide reversible interactions at low depletant concentrations. The specificity is a consequence of the geometry of the colloids, where the attraction between flat faces are favored by depletion interactions. We demonstrate that these interactions are transient, with survival times that depend on the shape of the interacting faces. The bond lifetime as a function of the depletant concentration is correctly predicted by a theoretical model based on excluded volume. We also show that the flat surfaces can slide relative to each other offering flexibility to the bonds. We quantify this sliding and show that it follows a Boltzmann distribution governed by the depletion energy. Bond breaking between surfaces occurred predominantly when they are offset relative to each other. Incorporating this flexibility on bond lifetime in our model yields a better quantitative agreement on the bond lifetimes. This quantification of specific, transient, and flexible bonds between simple anisotropic colloids could pave the way for the self-assembly of larger, defect-free colloidal structures.

1 Introduction

Colloidal self-assembly, leading to the formation of complex hierarchical end products is key to understand fundamental processes such as glass transition[1,2], crystallization[3–5], polymerization[6,7] etc. It also possesses application prospects in various scenarios such as preparation of photonic crystals[8], chemical sensing[9], biological applications[10] and many more[11,12]. At the heart of designing and organizing complex structures through self-assembly, lies the control of individual colloidal design and the mastery of their interactions. In various experimental attempts, researchers have demonstrated capability to tailor colloidal units that spontaneously self-assemble into intended structures based on chemical[13], geometrical[14–16], or physical cues[17–19]. Highly anisotropic colloidal interactions leading to the formation of directional bonds are achieved through altering the geometry, roughness and/or surface properties of colloids[20–23].

However, experimental achievement of the desired self-assembled structure is often hampered by kinetic trapping of the assembly, where too strong interactions leads to unorganized aggregate[24,25].

To build predictable aggregates from scratch, utilizing the principles of self-assembly, the building blocks and interactions should be carefully crafted to render the bonds (i) selective; that favor one type of assembly over another, (ii) reversible; that allow reorganizations of the large-scale structure, which helps to avoid kinetic traps in the energy landscape and (iii) flexible; that permits reconfiguration of the bonds between the building blocks[26,27] and allow for compensation of any defect in the manufacture of the individual particles.

Depletion interactions are ideally suited to induce colloidal self-

[a] PMMH, CNRS, ESPCI Paris, PSL University, Sorbonne Université, Université Paris-Cité, 75005, Paris, France
[b] Université Paris-Saclay, CNRS, LPTMS, 91405, Orsay, France.
[c] Present address: Department of Physics, Central University of Karnataka, India, 585367
[d] Gulliver, CNRS, ESPCI Paris, PSL University, Sorbonne Université, 75005, Paris, France

† Supplementary Information available: [details of any supplementary information available should be included here]. See DOI: 10.1039/cXsm00000x/

‡ Additional footnotes to the title and authors can be included *e.g.* 'Present address:' or 'These authors contributed equally to this work' as above using the symbols: ‡, §, and ¶. Please place the appropriate symbol next to the author's name and include a `\footnotetext` entry in the correct place in the list.

View Article Online
DOI: 10.1039/D5SM00841G

assembly. They can indeed be tuned independently of the colloid fabrication process and have been used to assemble lock-and-key particles through shape complementarity[15] Our goal in this work is to quantify how depletion interaction between flat surfaces simultaneously exhibit specificity, transience, and flexibility. Depletion interactions will take place between colloids in presence of non-adsorbing polymer , micelles, or other smaller colloidal particles. As the larger colloidal particles come into contact, the volume between them becomes inaccessible to the smaller entities and it is favorable in terms of entropy to push the larger colloids into close contact.[28,29]. For two colloids in contact over an area A, the binding free energy is proportional to $cA\delta$, with c being the depletant concentration and δ the range of interaction, which is proportional to the radius of gyration of the polymer, or the size of the smaller colloidal particle. Better fitting colloids with a larger area A benefit from stronger interaction, which accounts for the efficient binding of lock-and-key colloidal designs. The magnitude of depletion interactions has been experimentally verified for small colloids and non-ionic polymers through atomic force microscopy[30], surface force apparatus measurements[31,32], optical trapping[33] and total internal reflection microscopy[34,35]. One promising avenue to manufacture colloids with designed shapes, in addition to chemical synthesis and DNA origami[36], consists of 3D printing them on a substrate[37–41]. Two photon laser printing has recently been used to fabricate self-assembling colloids[16,42], offering a large design flexibility at the price of a lower throughput as compared to chemical routes. This approach enables the rational design and fabrication of highly anisotropic particles, ideally suited to create specific directional interactions. Using two-photon lithography, particles can be engineered with one or multiple flat surfaces. The overlapping excluded volume between two flat surfaces is much larger than the one between two spheres of the same dimension. Maintaining an attractive depletion energy of the order of a few k_BT to keep the transient property of the bond thus requires a much lower concentration of depletant compared to spheres, as low as a few entities by cubic microns. We used as depletant a polymer with a radius of gyration of approximately 50 which defines the range of the interaction. The absence of geometric interlocking between flat surfaces allows them to slide relative to one another, providing a route to reconfigurable reversible and flexible binding[43]. These features present both challenges and opportunities for depletion-driven self-assembly of two-photons lithography printed particles, that needs thorough investigation and quantification to obtain specific, transient, and flexible bonds for faithful large-scale complex self-assembly.

Here we conduct such an investigation using Brownian colloids produced by two-photon polymerization. We print colloids on a sacrificial polymer layer [44–46] to observe and quantify their in situ interactions. We chose a simple half-disk shape and induced depletion interactions through the addition of polyethylene glycol chains. The half-disk shape results in a stronger interaction through their vertical flat faces than their vertical rounded faces, quantified by the much longer lifetimes of the flat-flat interactions compared to flat-round and round-round. We observe and quantify sliding of half-disks interacting with their flat side, and show that separation between colloids mostly happens when colloids are offset relative to each other. We compare the survival times of the different interactions with increasing depletant concentration and satisfactorily model it assuming a simple Arrhenius kinetics. Incorporating the sliding-mediated pathway for bond dissociation yields a highly accurate prediction of the excluded volume. We anticipate that this quantitative framework will support the design of more complex self-assembling systems.

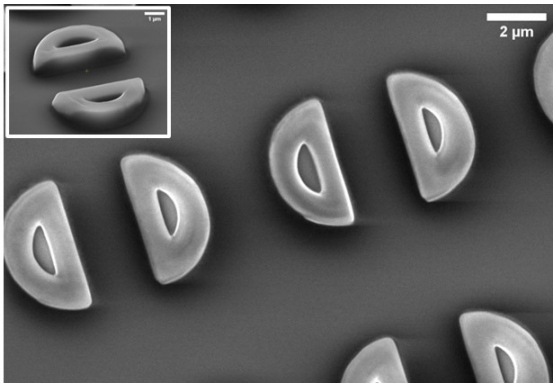

Fig. 1 Electron microscopy image showing the printed colloids, captured at an accelerating voltage of 15 kV. Inset: tilted image.

2 Methods

To obtain Brownian colloids with controlled shapes and number density, we 3D print the colloidal particles on a sacrificial layer of polyacrylic acid (PAA) (Sec.2.1). Once printed, we liberate the colloids by dissolving the layer, which allows them to diffuse and interact in situ, and control their interactions with depletion forces (Sec.2.2).

2.1 3D-printing of colloids.

Colloidal particles of half-disk shape are fabricated using 3D printing technique based on two-photon polymerization. To fabricate colloidal particles a sketch of the desired particle geometry is first made using a 3D designing software, Autodesk Inventor professional. Our colloids are designed to be semi-circular in shape with a diameter of 5μm and a height of 1μm. The particles are designed to be flat, in order to keep them parallel to the substrate during self-assembly, and to minimize particle flipping. The design is then loaded into the 'Describe' software linked to the 3D printer, Photonic professional GT from Nanoscribe, Germany. The 3D design is vertically sliced into parallel planes at fixed distances. Since the approximate height and diameter of a single voxel resulting from the tight focusing of laser onto the resist is 0.8 μm and 0.3 μm respectively, we maintain the vertical slicing and horizontal hatching distances at 0.2 μm during particle printing. This ensures optimal overlap between the neighboring voxels.

Colloids are printed in the conventional mode of direct-laser writing where the laser is focused through a thin glass substrate onto a photosensitive material (photo-resist). A circular cover glass of 30 mm diameter and 1.5 mm thickness is used as the substrate. After thorough oxygen plasma cleaning, we first coat the glass substrate with a thin layer of PAA using a 20mg/ml solu-

View Article Online
DOI: 10.1039/D5SM00841G

tion at 3000rpm for 30 seconds. A drop of IP-L photo-resist (from Nanoscribe GmbH, Germany) is placed on top of the PAA layer. The substrate is then loaded onto the 3D printer and the laser is focused onto the resist from underneath the glass substrate using a 63x oil-immersion objective (see Supporting Information Fig. S1 for a schematic). The laser then writes the 3D structures onto the photoresist. Since IP-L is a negative tone photoresist, the region where the laser impinges the photoresist is selectively reticulated to form colloidal particles. The unreacted photoresist is washed off using propylene glycol methyl ether acetate (Sigma Aldrich) leaving the printed colloidal particles on the substrate as the sacrificial PAA layer is insoluble in the developer solvent. Details about two-photon based $3D$ printing technique and the various process parameters to be optimized in the direct laser writing process may be found elsewhere[47,48]. A scanning electron microscopy (SEM) image of the printed particles is shown in Fig. 1. The printed semi-circular particles have a diameter $D = 4.60 \pm 0.05\,\mu$m as measured on SEM images and a height $h = 0.82 \pm 0.06\,\mu$m as inferred from optical microscopy measurements detailed in the supporting information (see Supporting Information Fig. S2). The hole in the middle of the colloids enables their easy detection and analysis in particular to measure the centroid and orientation (see Supporting Information Fig. S3).

2.2 Detachment of the particles from the printing substrate.

The printed particles are liberated from the substrate by dissolving the PAA sacrificial layer in a depletant solution that contains different chemicals dissolved in water: To induce depletion interactions and shape-selective binding between the printed colloids, we introduce polyethylene glycol (PEG) (MW 600 kDa, from Sigma Aldrich) with a radius of gyration of $50.2 \pm 1.5nm$ as the depletant. To prevent unfavorable and irreversible binding between colloids we use a non-ionic surfactant, tergitol at 20 ppm (from Sigma Aldrich), and salt at 50 mM (NaCl) to screen electrostatic repulsion between the printed colloids by decreasing the Debye screening length of the system.

Before dissolving the PAA layer to release the particles, we make a small chamber around the printed colloids to contain the solution and prevent fluid flow. A rubber 'O-ring' (internal diameter 3.4 mm, thickness 1.9 mm) is first fixed to the glass substrate around the printed colloids by using a thin layer of silicon oil. About $20\mu l$ of depletant solution is carefully placed inside the chamber, which is then sealed with a glass cover slip to avoid evaporation (see Supporting Information Fig. S4 for a schematic). The colloids are observed using an optical microscope from Carl Zeiss in bright field mode under 100x magnification using an oil-immersion objective. Time-lapse movies are acquired through a Michrome 6 CMOS camera (Keyence, France).

3 Results

After dissolution of the sacrificial layer, the colloids start to diffuse (Sec. 3.1) and upon contacting one another form bound pairs due to depletion interaction whose lifetimes (Sec. 3.2), fluctuations (Sec. 3.3) and breaking behaviour (Sec. 3.4) we characterize below alongside their dependence on the depletant concentration (Sec. 3.5).

3.1 Diffusion of individual particles.

As the depletant solution is administered into the chamber, the PAA sacrificial layer dissolves, allowing the printed particles to diffuse along the glass surface. Gently placing the depletant solution liberates the colloids without flipping them. The liberated particles remain close to the bottom of the chamber as a result of their higher density compared to water. As we show below, bonds form between the colloids and detach. In our movies that are acquired at least ten minutes after dissolution of the PAA layer, we can safely consider that the initial orientational order is completely randomized by thermal fluctuations (see Supporting Information figure S5). The geometric center of diffusing particles is tracked over time, to monitor their trajectories. By calculating the mean square displacement of the diffusing particles, we measure the diffusion coefficient of the individual colloidal particles to be equal to $0.044 \pm 0.002\,\mu\text{m}^2/\text{s}$, close to the theoretical estimate of $0.06\,\mu\text{m}^2/\text{s}$ (see Supporting Information Fig. S6). This diffusion is sufficient to cause several contacting events between neighboring colloids in the typical course of our experiments. We do not observe any appreciable out-of-plane fluctuations of the colloids.

3.2 Direct observation of transient bond formation and breakage.

Two colloids coming into contact can do so in three different configurations: their respective flat faces may come together, or their round ones, or they may incur a mixed flat-round contact. Fig. 2(A) shows the formation, temporal evolution, and breaking of the three types of bonds observed in our system at a depletant concentration of 0.01 mg/ml. The time at which bond formation takes place is denoted as t=0. In all three cases, individual colloids fluctuate with respect to each other. The flat-flat bonds are longest-lived, indicating that the bonds between colloids are shape-selective.

To further confirm the shape specificity of depletion interaction in our system, we observe several bound pairs of each category over 60 seconds and identify the time of bond breakage. The survival probability of each bond species is calculated using the following procedure. Each pair is continuously observed over a period of one minute to identify the time at which they fall apart. If a bond survives from time 0 to 25 sec within the one minute period, the life time of that particular bond is identified as 25 sec. Similar measurement is repeated on a minimum of 30 pairs in each bond configuration and a series of life times are obtained. A probability distribution curve is drawn with the obtained lifetimes which is termed as survival probability throughout this article. Fig. 2 (B) shows the survival probability of each of the three types of bonds at 0.01 mg/ml PEG. As expected, flat-flat bonds have a considerably higher survival probability compared to flat-round or round-round configurations,confirming that depletion forces are well suited to program directed interactions between colloids with flat faces.

View Article Online
DOI: 10.1039/D5SM00841G

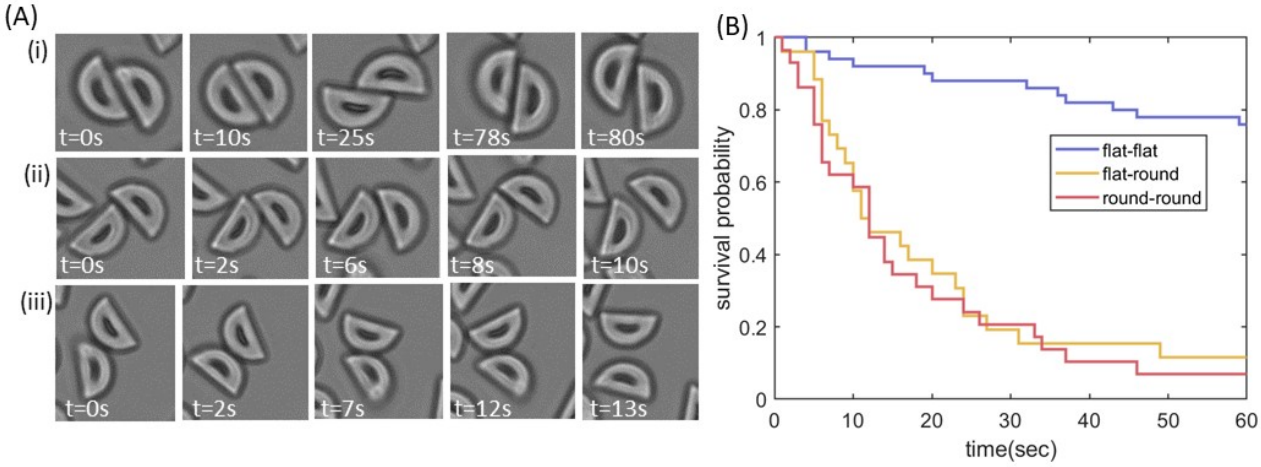

Fig. 2 The life time of a bond depends on its geometry. (A) Time lapse of bond formation, evolution and breaking between a pair of colloids in (i) flat-flat (ii) flat-round and (iii) round-round configuration. Note that the timescales (time is indicated on every image) vary a lot between the first row and the two others. (B) Survival probability of the three different types of bonds formed in the system, at a depletant concentration of 0.01 mg/ml PEG. The measurement is carried-out for a minimum of 30 pairs in each configuration.

3.3 Bond fluctuations.

To investigate the fluctuations of a single flat-flat bond, we plot the offset Δx between the adjacent edges of the two colloids as a function of time in Fig. 3(A). For each micrograph in our time series, we obtain the value of this offset by projecting the centroid of one of the ellipses to the major axis of the second ellipse, and then calculating the distance between the point of projection and the centroid of the second ellipse. When the flat faces of the two colloids are perfectly aligned with each other, the offset value is zero. The offset takes positive or negative values depending on the relative positions of two colloids while they fluctuate. The pair of colloids represented in Fig. 3(A) explores a range of Δx values ranging from -2μm to $+2\mu$m within the observation time of 60 seconds, and we show snapshots of the state of the bond at the times indicated by black dots. Despite this highly flexible nature, the bound pair spends most of its time in configurations close to $\Delta x = 0$, which have the lowest depletion free energy

To determine whether the fluctuations of the bond are consistent with our simplified picture of two perfectly flat faces constrained solely by depletion interactions, we follow 42 flat-flat bonds over 1 minute with a frame rate of 1 per second and plot the probability density function of $|\Delta x|$. Equilibrium thermodynamics predicts that this probability distribution should follow a Boltzmann distribution $p(\Delta x) \propto e^{-\Delta F/k_BT}$. The loss of free energy, ΔF, here reads $\Delta F = k_BTc\Delta V$ for a loss of excluded volume $\Delta V = 2\delta h|\Delta x|$ with c the depletant concentration, h, the particle height and δ, the thickness of the depletion layer. This thickness sets the range of depletion interaction which reads for polymeric depletant by $\delta = 2R_g/\sqrt{\pi}$, where R_g is the radius of gyration of the polymer[49]. For PEG 600kDa used in this study, $R_g = 50.2 \pm 1.5nm$[50]. The probability distribution of $|\Delta x|$ can be rewritten as $p(\Delta x) = \lambda^{-1}e^{-|\Delta x|/\lambda}$ with $\lambda = (2h\delta c)^{-1}$. Using $c = XXX$, $h = 0.82\mu$m, we obtain a theoretical prediction of $\lambda_{th} = (2h\delta c)^{-1} = 1.07 \pm 0.08\mu m$. The experimental data shown in Fig. 3(B) are consistent with this prediction and their fit gives an estimate of $\lambda = 0.80 \pm 0.04\mu m$. The difference between prediction and measurement may be due to the friction between the two surfaces, which is unaccounted for here. This model suggests that bonds are mostly observed in configurations whose depletion free energy is within k_BT of its minimum value. Consistent with this expectation, our bonds rarely display very large values for $|\Delta x|$ despite remaining dynamic.

3.4 Bond breaking.

While bond configurations with large values of $|\Delta x|$, are rare, we expect that they would be the most likely to break apart due to the small overlap of the half-disks. To assess the kinetic pathway leading to bond breakage, we measure the angle θ between the major axes of the elliptical fits of the two particles. When the particles are bound, the two flat faces stay parallel to each other, making an angle between the two ellipses close to 0°. However, sometimes the angle between the major axes abruptly increases (see Supporting Information Fig. S7) and the particles separate. In this case, we record the corresponding bond breaking time, and $|\Delta x|$ value.

We show the time evolution of the offset $|\Delta x|$ for 7 flat-flat bonds in Fig. 4(A), with time 0 indicating their breakage. We observe that breakage tends to occur for relatively high offsets. To confirm this observation, we summarize the behaviour of 42 flat-flat pairs in Fig. 4(B). In this figure, each column shows the different values of $|\Delta x|$ (black dots) explored by a pair during the course of an experiment (one minute). The value at which the pair breaks, if it exists, is represented by a red circle. The pairs are ranked horizontally on the basis of their highest value $|\Delta x|$. The first observation of this figure reveals that a pair can explore offset values greater than the one at which it - or the others - breaks, reminding us that the phenomenon we are studying is stochastic because it is induced by thermal fluctuations. Second, three different regions are visible corresponding to different offset ranges. Although all pairs visit the low offset region, (I), no bond breakages are observed there, which is consistent with an associated

View Article Online
DOI: 10.1039/D5SM00841G

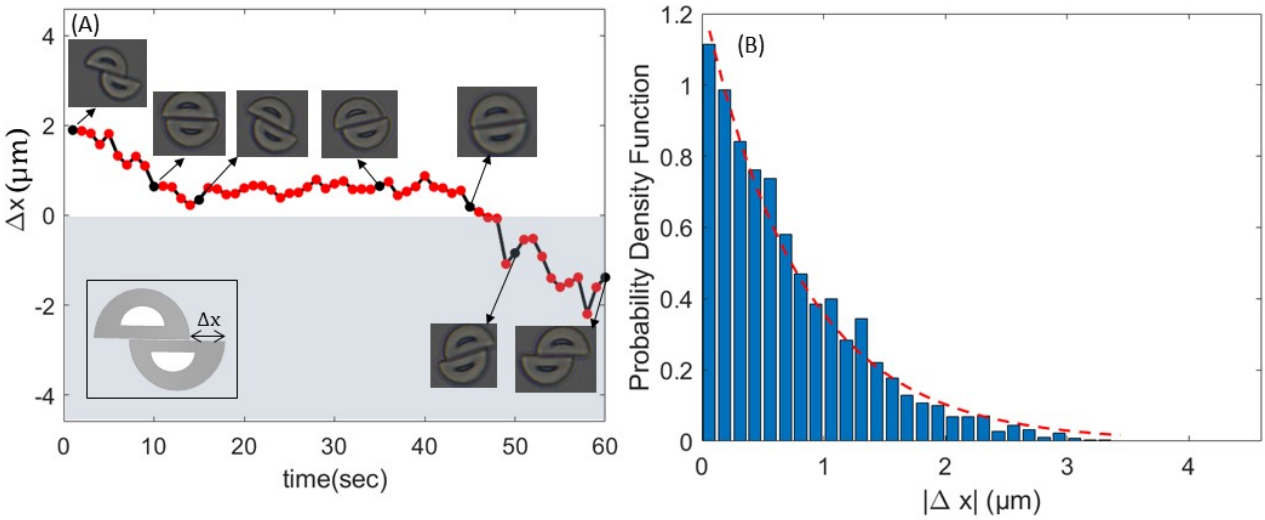

Fig. 3 Bond fluctuations are consistent with those of an equilibrium steady state.(A) Temporal evolution of the offset Δx schematized in the inset between the adjacent edges of colloids showing the fluctuation of a bond in flat-flat configuration. (B) Probability density function corresponding to the occurrence of $|\Delta x|$ values during fluctuation of bonds in flat-flat configuration formed by the depletion-assisted association of semi-circular colloids at a depletant concentration of 0.01mg/ml, with exponential fit (red dotted line) superimposed.

binding free energy that is large relative to the thermal energy (in excess of $3k_BT$) leading to a very favorable binding. All observed breakage events occur in region II, which corresponds to a binding free energy comprised between 1.2 and $3k_BT$, low enough to be overcome by thermal fluctuations over the time scale of our observations. Finally, none of our bonds explores the high-offset region III, which would correspond to very weak bonds. In the next section, we investigate how these behaviours are affected as we alter the bond energy by changing the concentration of depletant.

3.5 Influence of the depletant concentration.

We investigate the effect of depletant concentration on the decay and breaking behaviour of various bonds formed in our system. Firstly, we assess the survival probability of colloidal pairs in the three different bond configurations viz flat-flat, flat-round, round-round formed at various depletant concentrations (0.02 mg/ml, 0.015 mg/ml, 0.01 mg/ml and 0.008 mg/ml PEG) (see Fig. 5). To obtain a quantitative estimation of the bond lifetime τ, we fit the survival probabilities with a decreasing exponential as a function of time ($p = e^{-t/\tau}$). As expected for depletion interactions, the survival probability of each type of bonds decreases as the strength of depletion interaction is lowered, but the specificity of the interaction with flat-flat much stable than the other configurations is maintained in the range tested here. Fig. 5 shows the survival probability of each type of bonds as a function of depletant concentrations. In the absence of any added depletant, the colloidal particles do not form stable bonds: any two colloidal particles that approached each other randomly, diffused away spontaneously within 1-2 seconds, indicating the absence of stable bond formation.

Furthermore, to interrogate the relationship between depletant size to the life time of our bonds, we conduct experiments with a larger depletant(2000 kDa PEG) with approximately double the gyration radius of the original one (114 nm). The concentration of depletant is set at 0.02 mg/ml, which corresponds to $-5.2k_BT$ depletion interaction strength on perfect flat-flat alignment of two colloids. The survival probability of flat-round and round-round pairs formed in presence of 0.02mg/ml 2000kDa PEG is shown in the supporting information (see Fig S10 in the supporting information. The measured survival times(tabulated in table1) lie between the survival times obtained in similar configurations formed with 600kDa PEG at concentrations that results in flat-flat bond energy close to $-4.29k_BT$(0.01 mg/ml) and $-6.44k_BT$(0.015 mg/ml). A similar comparison of flat-flat bond life times is not possible due to experimental limitations while using large depletant, leading to slower diffusion of colloids and their immobilization within 10-15 minutes of the start of the experiment (see supplementary information for details).

In a first approach, to compare the survival times to classical theory of depletion we assimilate bond breakage to the escape from a single potential well of depth ΔF, where ΔF denotes the depletion free energy associated with a bond configuration. According to Kramers theory, the survival probability of the bond should then follow the type of exponential decay described above, with a mean detachment time given by the Arrhenius law $\tau = \tau_0 e^{\Delta F/k_BT}$, where τ_0 is a constant typical diffusion time scale for the problem. ΔF is given by the product of the osmotic pressure and the change in excluded volume ΔV yielding $\Delta F = k_BTc\Delta V$. We thus obtain a simple prediction for the survival probability $\ln(\tau) = \ln(\tau_0) + c\Delta V$. We then fit the three curves of τ as a function of concentration with four parameters, ΔV for each configuration (flat-flat, flat-round and round-round) and the same pre-exponential constant τ_0. These values are very close to a geometric estimate of the excluded volume change for each of the bond configurations (see Table 2 and supplementary data for calculation).

View Article Online
DOI: 10.1039/D5SM00841G

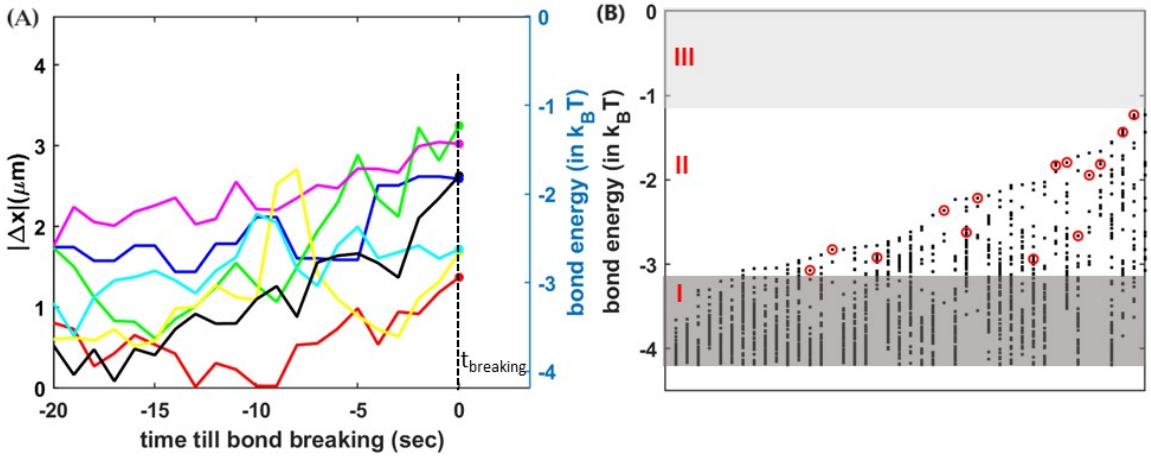

Fig. 4 Bond breaking dynamics of flat-flat pairs: (A) Temporal evolution of $|\Delta x|$ recorded from 20 seconds prior to breakage of the bond till the breaking time, $t_{breaking}$ corresponding to 7 different flat-flat pairs formed at a depletant concentration of 0.01 mg/ml (left Y-axis) and the corresponding bond energies in units of k_BT (right Y-axis). The $|\Delta x|$ at $t_{breaking}$ is denoted by filled circles for each pair. (B) Bond energy values explored by various pairs of colloids in flat-flat configuration at 0.01 mg/ml depletant concentration. The bond energies at breaking is indicated by red open circles. The region marked with I, II and III are indicative of the limit within which the colloidal bonds are stable against breaking, transient, and unstable respectively. Out of the 42 bonds represented here, 14 bond breaking events are observed.

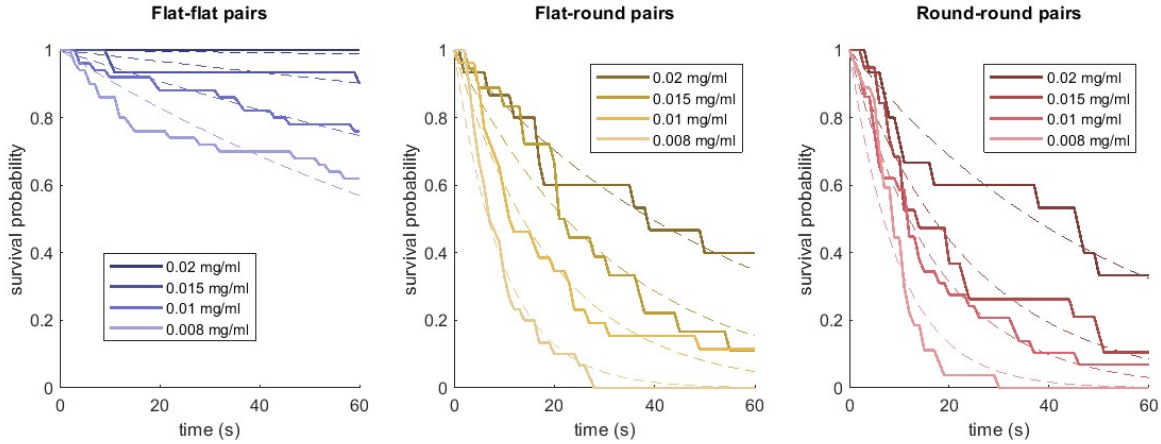

Fig. 5 Dependence of survival probability of the three types of bonds in (i) flat-flat (ii)flat-round and (iii) round-round configurations for four different concentration of PEG depletant. Dashed lines: fit to obtain the survival times.

3.6 Influence of sliding on the bond lifetime.

Despite this good agreement, we speculate that the deviations of our fitted values from our geometrical estimates could stem from the flexibility of the flat-flat bonds. Indeed, as the flat surfaces of two bound colloids randomly slide off of a perfect alignment due to thermal fluctuations, they reduce the overlap of their excluded volume. This increases the rate of their detachment, and potentially offers a fast, "slide-then-break" kinetic pathway towards bond breakage. This hypothesis is supported by the observation of the flat-flat detachment scenario showing sliding at the 4 different depletant concentrations studied (SI Fig. S9). Although detachment occurs at all offsets at the lower depletant concentration and is not observed at the highest concentration, at intermediate concentrations, detachment occurs only for the highest offsets. Plotting the detachment scenario with the calculated bond energy instead of the offset, a qualitative agreement is obtained with (SI Fig. S9), where all flat-flat pair separations occurs between an energy of $-4kT$ to $-1kT$.

Beyond this qualitative observation, we aim to validate our slide-then-break hypothesis by modeling it quantitatively. For a shift Δx, the binding free energy between the colloids is reduced by an amount $2k_BTch\delta|\Delta x|$. By assuming a simple Arrhenius kinetics for their detachment, we thus predict a detachment rate $k(\Delta x) = \tau_0^{-1}\exp[cV(\Delta x)]$, where the overlap between the colloids' depletion volumes is given by $\Delta V = 2h\delta(R-|\Delta x|)$. Using the probability $p(\Delta x)$ derived in Sec. 3.3, we compute the mean colloid detachment rate $K = \int p(\Delta x)k(\Delta x)\,\mathrm{d}\Delta x$. Defining the effective overlap ΔV_{eff} between the two colloids through $K = \tau_0^{-1}\exp(c\Delta V_{\mathrm{eff}})$, our calculation yields

$$c\Delta V_{\mathrm{eff}} = cV_M + \ln\left(\frac{1-e^{-c\Delta V_M}}{c\Delta V_M}\right), \qquad (1)$$

where the maximum overlap is given by $\Delta V_M = \Delta V(\Delta x = 0)$. We then fit again (see Fig. 6) using this modified model the ensemble of the three variations of τ as a function of concentration,

View Article Online
DOI: 10.1039/D5SM00841G

MW(PEG)	concentration(mg/ml)	$E_{f-f}(k_BT)$	τ_{f-f}	τ_{f-r}	τ_{r-r}
600 kDa	0.02	-8.59	6045 ± 1567	56.88 ± 2.14	53.19 ± 3.04
	0.015	-6.44	584.8 ± 61.2	32.04 ± 1.94	24.29 ± 1.26
	0.010	-4.29	205.5 ± 5.6 19.78 ± 0.90	17.23 ± 0.52	
	0.008	-3.43	106.4 ± 6.5	9.75 ± 0.57	9.86 ± 0.92
2000 kDa	0.020	-5.20	–	20.2 ± 1.3	13.59 ± 0.78

Table 1 The average survival time of different bonds obtained through exponential fitting

	flat-flat	flat-round	round-round
ΔV from geometry (μm^3)	0.426 ± 0.032	0.089 ± 0.007	0.063 ± 0.005
ΔV from Arrhenius (μm^3)	0.338	0.118	0.109
ΔV from Arrhenius with sliding (μm^3)	0.462	0.106	0.097

Table 2 Excluded volume change when two particles contact, calculated from the geometry of the particle and compared with estimates derived from fits of the survival time as a function of concentration.

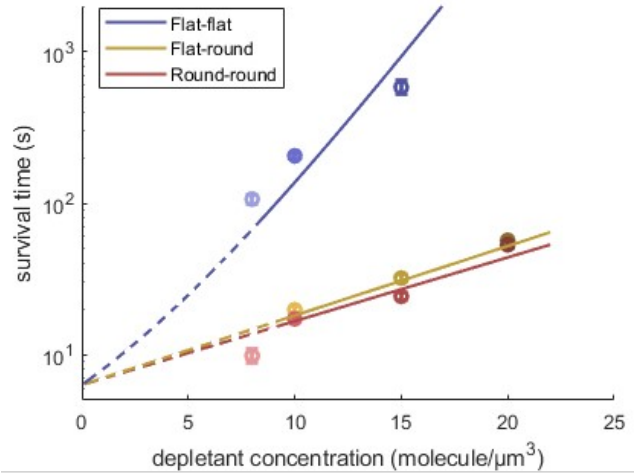

Fig. 6 Survival time as a function of depletant concentration (PEG 600 kDa) for the flat-flat, flat-round and round-round configurations, with associated fits of Arrhenius law, modified in the flat-flat case for reduced survival associated with sliding.

to obtain an estimation of ΔV_M for flat-flat, and a new estimate of ΔV for flat-round and round-round configuration.The results are shown in Table2 and show a much better agreement with the geometric estimates. This better agreement supports our slide-then-break kinetic model, and thus demonstrates that depletion forces can adequately explain the dynamics of aggregation of these micro-fabricated colloids and that other attractive forces, such as van der Waals interaction, only plays a minor role.

4 Discussion

Successfully self-assembling particles into a predetermined structure involves two challenges. On the one hand, the target structure should be more stable than its competitors. On the other, it must be kinetically accessible. While 3D-printed microparticles offer a remarkable flexibility in achieving complex stable structures, kinetic accessibility is potentially problematic at their relatively large scale, where diffusion is much slower than in, e.g., DNA origami. This difficulty can however be offset by a fine control over the interactions between the particles, e.g., allowing off-target bonds to quickly detach, while even favorable ones are allowed to occasionally come off to allow the particles to optimize their large-scale arrangement.

In this study, we have demonstrated an experimental strategy to achieve such control. We implement reversible bonding with a life time directly controlled by the particles' shapes, demonstrating that 3D printing can be used to not only control an aggregate's morphology, but also its dynamics. Since the strength of our bonds is controlled both through the depletant concentration and the contact area between the colloids, our design can straightfowardly be generalized to generate a system where different bonds have different lifetimes. This potentially opens the possibility to use 3D printing to design structures based on hierarchical self-assembly, which take advantage of the existence of several scales of bond life time and strength to reliably assemble complex structures. We also demonstrate that the spatial control afforded by 3D printing can be harnessed to generate flexible aggregates whose rigidity is controlled by easily controlled deple-

View Article Online
DOI: 10.1039/D5SM00841G

tion interactions. While such sliding of flat colloid surfaces in the presence of depletion attraction have previously been observed with silica cubes[51], ours is to our knowledge the first implementation of this effect in a 3D-printed self-assembled system. On larger scales, this sliding can in principle be controlled through the size of the depletant, an effect that has previously been used to select between different lattice organisations[14].

In addition to allow for the implementation of non-rigid self-assembled structures, we demonstrate that the flexibility of a bond has a direct influence over its lifetime through a slide-then-break mechanism, allowing one more lever to control the dynamics of colloidal self-assembly by taking advantage of the spatial control afforded by 3D-printing. While our study concentrates on the dynamics of a single inter-colloid bond, we anticipate that our design can easily be scaled up to generate particles with multiple binding sites. As this strategy opens the way to much more complex designs, flexibility could prove an asset in yet another way. Specifically, in such a context bond flexibility could compensate for imperfections in the colloids' shapes, by allowing, e.g., a ring of particles each carrying two bonds at an angle to one another to close even in cases where these angles are not exactly adjusted. We thus anticipate that the tool box developed here could open the range of possible designs for the self-assembly of 3D-printed objects, both in the quasi-two-dimensional setting considered here and in future 3-dimensional situations.

5 Acknowledgments

This work was supported by the "Défi Auto-Organisation" of CNRS' mission of transverse and interdisciplinary initiatives and ANR grant (ANR-22-CE30-0024). ML was supported by ERC Starting grant 677532, ANR's Tremplin ERC grant ANR-21-CE11-0004-02 the Impulscience® program of Fondation Bettencourt Schueller. The 3D printer setup was acquired through SESAME Region Ile de France MiLaMiFab grant. OdR and JH are members of GDR 2108 Quantitative approach of Life.

Notes and references

1 E. R. Weeks, J. C. Crocker, A. C. Levitt, A. Schofield and D. A. Weitz, Science, 2000, **287**, 627–631.
2 E. R. Weeks and D. A. Weitz, Chemical physics, 2002, **284**, 361–367.
3 Y. Wang, Y. Wang, X. Zheng, É. Ducrot, J. S. Yodh, M. Weck and D. J. Pine, Nature communications, 2015, **6**, 7253.
4 P. N. Pusey and W. Van Megen, Nature, 1986, **320**, 340–342.
5 V. J. Anderson and H. N. W. Lekkerkerker, Nature, 2002, **416**, 811–815.
6 A. McMullen, M. Holmes-Cerfon, F. Sciortino, A. Y. Grosberg and J. Brujic, Physical review letters, 2018, **121**, 138002.
7 B. Luo, J. W. Smith, Z. Wu, J. Kim, Z. Ou and Q. Chen, ACS nano, 2017, **11**, 7626–7633.
8 Z. Cai, Z. Li, S. Ravaine, M. He, Y. Song, Y. Yin, H. Zheng, J. Teng and A. Zhang, Chemical Society Reviews, 2021, **50**, 5898–5951.
9 J.-T. Zhang, L. Wang, J. Luo, A. Tikhonov, N. Kornienko and S. A. Asher, Journal of the American Chemical Society, 2011, **133**, 9152–9155.
10 Y.-C. Kuo and C.-C. Lin, Colloids and Surfaces B: Biointerfaces, 2013, **103**, 595–600.
11 Z. Li, Q. Fan and Y. Yin, Chemical reviews, 2021, **122**, 4976–5067.
12 J. Ge and Y. Yin, Angewandte Chemie International Edition, 2011, **50**, 1492–1522.
13 M. He, J. P. Gales, X. Shen, M. J. Kim and D. J. Pine, Langmuir, 2021, **37**, 7246–7253.
14 S. Sacanna, D. J. Pine and G.-R. Yi, Soft Matter, 2013, **9**, 8096.
15 S. Sacanna, W. T. Irvine, P. M. Chaikin and D. J. Pine, Nature, 2010, **464**, 575–578.
16 T. Tigges and A. Walther, Angewandte Chemie International Edition, 2016, **55**, 11261–11265.
17 B. Bharti, F. Kogler, C. K. Hall, S. H. Klapp and O. D. Velev, Soft Matter, 2016, **12**, 7747–7758.
18 A. Van Blaaderen, Mrs Bulletin, 2004, **29**, 85–90.
19 J. Dobnikar, A. Snezhko and A. Yethiraj, Soft Matter, 2013, **9**, 3693–3704.
20 W. Li, H. Palis, R. Mérindol, J. Majimel, S. Ravaine and E. Duguet, Chemical Society Reviews, 2020, **49**, 1955–1976.
21 Watanabe, Kanako and Tajima, Yui and Shimura, Takuya and Ishii, Haruyuki and Nagao, Daisuke, Journal of Colloid and Interface Science, 2019, **534**, 81–87.
22 Watanabe, Kanako and Shimura, Takuya and Nagasawa, Akira and Nagao, Daisuke, Langmuir, 2021, **37**, 9451–9456.
23 Badaire, Stéphane and Cottin-Bizonne, Cécile and Stroock, Abraham D, Langmuir, 2008, **24**, 11451–11463.
24 Jankowski, Eric and Glotzer, Sharon C, Soft Matter, 2012, **8**, 2852–2859.
25 Klotsa, Daphne and Jack, Robert L, Soft Matter, 2011, **7**, 6294–6303.
26 Chakraborty, Indrani and Pearce, Daniel JG and Verweij, Ruben W and Matysik, Sabine C and Giomi, Luca and Kraft, Daniela J, ACS nano, 2022, **16**, 2471–2480.
27 Ortiz, Daniel and Kohlstedt, Kevin L and Nguyen, Trung Dac and Glotzer, Sharon C, Soft Matter, 2014, **10**, 3541–3552.
28 S. Asakura and F. Oosawa, The Journal of chemical physics, 1954, **22**, 1255–1256.
29 L. Colón-Meléndez, D. J. Beltran-Villegas, G. Van Anders, J. Liu, M. Spellings, S. Sacanna, D. J. Pine, S. C. Glotzer, R. G. Larson and M. J. Solomon, The Journal of chemical physics, 2015, **142**, 174909.
30 Milling, Andrew and Biggs, Simon, Journal of Colloid and Interface Science, 1995, **170**, 604–606.
31 M. Ruths, H. Yoshizawa, L. J. Fetters and J. N. Israelachvili, Macromolecules, 1996, **29**, 7193–7203.
32 T. L. Kuhl, A. D. Berman, S. W. Hui and J. N. Israelachvili, Macromolecules, 1998, **31**, 8250–8257.
33 J. C. Crocker, J. A. Matteo, A. D. Dinsmore and A. G. Yodh, Physical review letters, 1999, **82**, 4352.
34 D. Rudhardt, C. Bechinger and P. Leiderer, Physical review

View Article Online
DOI: 10.1039/D5SM00841G

letters, 1998, **81**, 1330.
35 T. D. Edwards and M. A. Bevan, Langmuir, 2012, **28**, 13816–13823.
36 T. Tigges, T. Heuser, R. Tiwari and A. Walther, Nano letters, 2016, **16**, 7870–7874.
37 A. Brown, C. Smith and A. Rennie, Physical Review E, 2000, **62**, 951.
38 T. J. Merkel, K. P. Herlihy, J. Nunes, R. M. Orgel, J. P. Rolland and J. M. DeSimone, Langmuir, 2010, **26**, 13086–13096.
39 C. J. Hernandez and T. G. Mason, The Journal of Physical Chemistry C, 2007, **111**, 4477–4480.
40 J. H. Moon, A. J. Kim, J. C. Crocker and S. Yang, Advanced Materials, 2007, **19**, 2508–2512.
41 J.-H. Jang, C. K. Ullal, S. E. Kooi, Koh and E. L. Thomas, Nano letters, 2007, **7**, 647–651.
42 R. P. Doherty, T. Varkevisser, M. Teunisse, J. Hoecht, S. Ketzetzi, S. Ouhajji and D. J. Kraft, Soft Matter, 2020, **16**, 10463–10469.
43 L. Rossi, S. Sacanna, W. T. Irvine, P. M. Chaikin, D. J. Pine and A. P. Philipse, Soft Matter, 2011, **7**, 4139–4142.
44 C. J. Hernandez and T. G. Mason, The Journal of Physical Chemistry C, 2007, **111**, 4477–4480.
45 J. W. Tavacoli, P. Bauër, M. Fermigier, D. Bartolo, J. Heuvingh and O. du Roure, Soft Matter, 2013, **9**, 9103–9110.
46 Y. C. Saraswat, F. Ibis, L. Rossi, L. Sasso, H. B. Eral and P. Fanzio, Journal of Colloid and Interface Science, 2020, **564**, 43–51.
47 A.-I. Bunea, N. del Castillo Iniesta, A. Droumpali, A. E. Wetzel, E. Engay and R. Taboryski, Micro, 2021, pp. 164–180.
48 Zhou, X and Hou, Y and Lin, J, AIP Adv. , 2015, **5**, 030701.
49 G. J. Fleer, A. M. Skvortsov and R. Tuinier, Macromolecules, 2003, **36**, 7857–7872.
50 K. Devanand and J. Selser, Macromolecules, 1991, **24**, 5943–5947.
51 L. Rossi, S. Sacanna, W. T. M. Irvine, P. M. Chaikin, D. J. Pine and A. P. Philipse, Soft Matter, 2011, **7**, 4139–4142.

View Article Online
DOI: 10.1039/D5SM00841G

Data for this article are available at https://dropsu.sorbonne-universite.fr/s/4EyNEcCdpr5GMFg.